

Transportmetrica B: Transport Dynamics

ISSN: (Print) (Online) Journal homepage: www.tandfonline.com/journals/ttrb20

Recalibration of the BPR function for the strategic modelling of connected and autonomous vehicles

Esta Qiu, Navreet Virdi, Hanna Grzybowska & Travis Waller

To cite this article: Esta Qiu, Navreet Virdi, Hanna Grzybowska & Travis Waller (2022) Recalibration of the BPR function for the strategic modelling of connected and autonomous vehicles, *Transportmetrica B: Transport Dynamics*, 10:1, 779-800, DOI: [10.1080/21680566.2022.2040063](https://doi.org/10.1080/21680566.2022.2040063)

To link to this article: <https://doi.org/10.1080/21680566.2022.2040063>



Published online: 28 Feb 2022.



Submit your article to this journal



Article views: 684



View related articles



View Crossmark data



Citing articles: 6 View citing articles



Recalibration of the BPR function for the strategic modelling of connected and autonomous vehicles

Esta Qiu^a, Navreet Virdi^a, Hanna Grzybowska  ^b and Travis Waller  ^a

^aSchool of Civil and Environmental Engineering, University of New South Wales, Sydney, Kensington, Australia;

^bData61, CSIRO Level 5, Eveleigh, Australia

ABSTRACT

This paper assesses the adequacy of the BPR volume delay function for the strategic modelling of Connected and Autonomous Vehicles (CAVs). Three testbed environments are simulated at 10% increments of CAV penetration rates (CPR) to observe network performance in mixed fleet environments. The microsimulation dataset is compared with the BPR travel time predictions to evaluate the need for recalibration. Where appropriate, the BPR modelling parameters are redefined as a function of the CPR. The predictive quality of the recalibrated model is then validated by comparing it against the BPR function on synthetic data. The numerical results indicate an overall improvement in travel time prediction using the recalibrated model, with a significant reduction in root mean square error from 15.16 to 8.86. The recalibrated model also outperformed the traditional BPR model in 67% of the 4620 cases used for validation, and better-predicted travel time by 5.43 times.

ARTICLE HISTORY

Received 30 July 2020

Accepted 3 February 2022

KEYWORDS

Connected and autonomous vehicles; volume delay function; strategic modelling; microsimulation

1. Introduction

Connected and Autonomous Vehicles (CAVs) are being explored in great detail by academics, governments, and the private sector, as they pose a means of mitigating congestion, improving transport systems efficiency, or forming a lucrative new venture (Clements and Kockelman 2017). Follow-on benefits include positive economic growth and productivity gains from saved driving time and labour (Clements and Kockelman 2017), or potentially repurposing infrastructure such as parking lots and street parking space (Heinrichs 2016). As the technology moves from concept to development, significant research is being conducted into the potential implications of CAVs for society such as network reaction, use behavioural changes, or necessary infrastructure and policy alterations. Strategic transport modelling is a vital resource in evaluating the impact of this quickly emerging technology.

Transport modelling is critical in infrastructure-planning and traffic management. Currently, all transport management and control measures are based on traffic behaviour generated by human drivers (Tettamanti, Varga, and Szalay 2016) and do not consider the impact of CAVs on network performance. For example, the Sydney Strategic Travel Model is a State-owned city planning model that only considers modes of travel by car, rail, ferry, bus, cycle and walk, and a combination thereof (Bureau of Transport Statistics NSW 2012), failing to include future and emerging technology such as CAVs. Many proposed CAV behavioural models rely on changing behavioural parameters such as sight distance, minimum acceptable gap, and lane change preferences (Tettamanti, Varga, and Szalay 2016;

CONTACT Esta Qiu  e.qiu@unsw.edu.au  School of Civil and Environmental Engineering, University of New South Wales, Sydney, High Street, Kensington, NSW 2052, Australia; Navreet Virdi  n.virdi@unsw.edu.au School of Civil and Environmental Engineering, University of New South Wales, Sydney, High Street, Kensington, NSW 2052, Australia

Xiangjun et al. 2015; Kamal et al. 2013; Antoniottiz, Deshpandez, and Giraultx 1997). Such attempts do not appropriately capture the intricate and complex effects that CAV behaviour has on network performance, nor is changing these parameters appropriately reflected in other models and algorithms of the strategic modelling platform such as volume delay functions (VDFs), junction delay functions, value of time, or choice parameters.

Strategic models often contain predefined parameters calibrated against local traffic data to capture field characteristics. The current suggested values for these parameters may be inappropriate for use with CAVs, as they were calibrated against localised historical data generated by human drivers. Simulation results suggest that 50% of total travel time can be reduced by equipping 80% of vehicles with Vehicle to Everything (V2X) communication (Katsaros et al. 2011). The same study demonstrated that CAVs can increase intersection throughput by 110%, reduce intersection delays by 63%, and reduce queue lengths by 28%. With the same traffic volume, the network delay induced by CAVs is lower than that of conventional vehicles, and the use of current strategic models may over-predict travel time. Travel time is a major contributing factor to vehicle routing in strategic models, the gross miscalculation of which, would render strategic models unusable.

The purpose of this paper is to investigate validity in the continued use of the BPR VDF as part of the strategic modelling practices when emulating networks with CAVs. Although many studies explored the implications of CAVs on transport planning (Epting 2019; Beza and Zefreh 2019; Harper et al. 2016), the impacts are discussed more conceptually than empirically.

The remainder of this paper is as follows. Section two reviews currently used VDFs and new strategic models proposed for CAVs. Section three presents the recalibration framework, the CAV emulation algorithm, as well as the microsimulation environments and scenarios used to synthesise data. Section four presents the results of this study, which includes the microsimulation results, as well as the mathematical predictions using the original strategic models and the recalibrated models. Section five provides a discussion of the attained results, and section six concludes the final findings.

2. Background

Transport modelling is an invaluable resource that helps inform governments of travel behaviour changes on a citywide scale, as a consequence of policy change or investment in civil transport infrastructure. The four-step model is a widely-used demand forecast model which estimates future travel behaviour and network performance and patronage on the network. This modelling process relies on developing a generalised cost function for each link and node in the network. By summing discretised link and node costs, a total path cost between origin-destination pairs is determined. The generalised path costs of competing routes are then equilibrated by adjusting vehicle routing (Saw, Katti, and Joshi 2015). Link delays and node delays are contingent on a range of factors including capacity, volume, heavy vehicle proportions, behavioural parameters, and localised parameters.

The specific cost function for links addressed in this study is the BPR VDF, explained in greater detail in Section 2.1. To contextualise the use and significance of the BPR function, refer to Figure 1. Capacity is often a variable required by most VDFs, and so methods for determining link capacity are investigated in Section 2.2. Section 2.3 outlines recent developments in strategic modelling for CAVs.

2.1. Commonly used Volume Delay Functions

VDFs describe the relationship between the travel cost of a road link and the traffic volume. VFDs are designed to mimic the deterioration in link travel speed as link volume increases. The standard BPR function was developed by the US Bureau of Public Roads in the 1960s, and is defined as (Bureau of Public Roads 1964):

$$t = t_0 \left(1 + \alpha \left(\frac{V}{C} \right)^\beta \right) \quad (1)$$

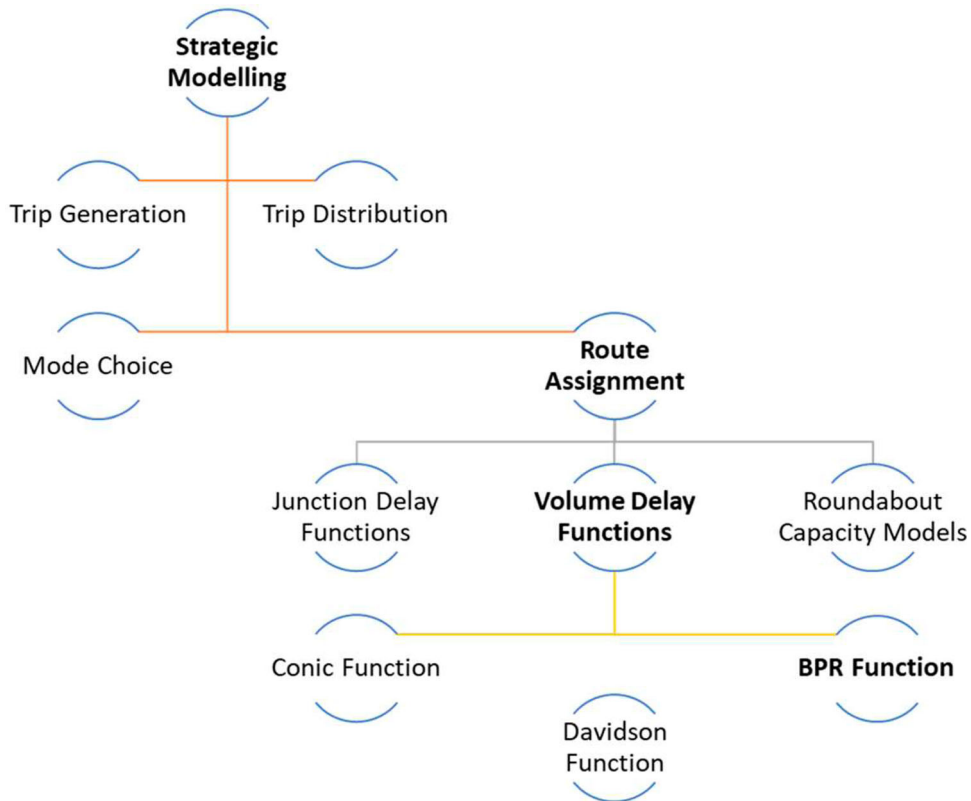


Figure 1. Contextualisation of the BPR function within the wider strategic modelling framework.

where t is the travel time (or cost) of the studied road link, t_0 is the travel cost under free-flow conditions, $\frac{V}{C}$ is the volume to capacity ratio also referred to as the degree of saturation (DoS), and α and β are calibration parameters that are unique to road geometry and environment.

The function was developed by fitting a polynomial equation to a freeway speed-flow curves observed on a single motorway in the United States (Highway Capacity Manual 2000). It is the most widely used function in transport modelling due to its simplicity and minimal input requirements (Mtoi and Moses 2014). Parameters α and β determine the shape of the function, with values often predefined based on assumptions and the characteristics of the network. α regulates the magnitude of the travel time increase relative to volume increase. β controls the rate at which the link cost increases with the flow, to reach the magnitude defined by α . Higher values of α indicate that conditions on a particular link become much worse with increasing traffic volume, while higher values of β indicate that the road is unable to absorb the effects of increasing traffic, and congestion effects become prominent sooner. Refer to Figure 2 for a diagrammatic representation of the influence of α and β .

The Conical Volume Delay Function (Spiess 1990) was introduced as an alternative to the BPR function and is defined as:

$$t = t_0 \left[2 + \sqrt{\alpha^2 \left(1 - \frac{V}{C}\right)^2 + \beta^2} - \alpha \left(1 - \frac{V}{C}\right) - \beta \right] \quad (2)$$

where the variables are consistent with the BPR function presented in Equation (1), but $\alpha > 1$ and $\beta = \frac{2\alpha-1}{2\alpha-2}$.

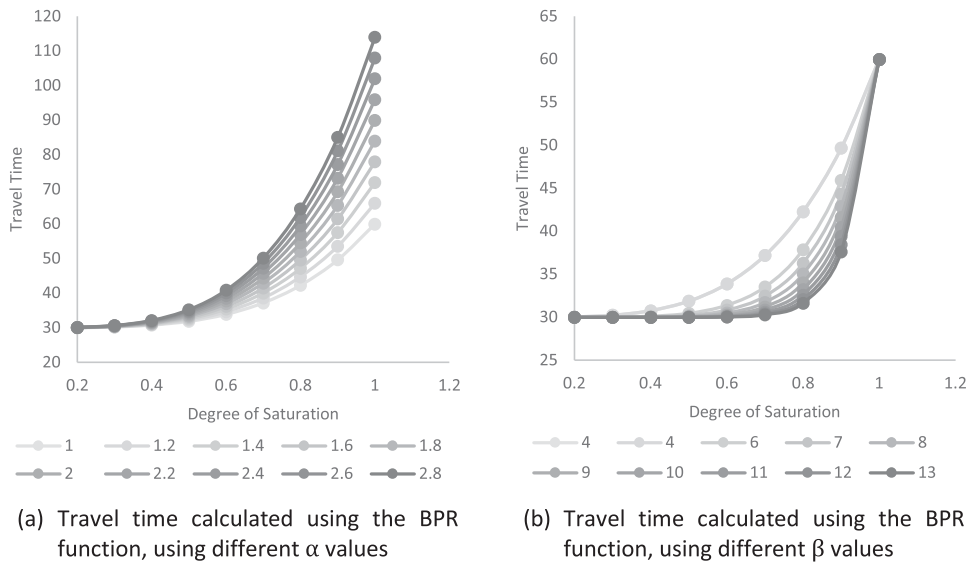


Figure 2. Impact of the α and β parameters on computed travel time using the BPR function.

The Conical Volume Delay Function addresses the inherent drawbacks of the BPR function, where a high exponent β value could lead to overflow conditions and loss of precision (Spiess 1990). High values of β in the BPR functions assign an undue weight to overloaded links during the first few iterations of an equilibrium assignment, which can cause numerical problems.

Davidson developed the Davidson Function in 1966 based on principles of queuing theory (Davidson 1978). The function is defined as:

$$t = t_0 \left(1 + \frac{J_d \cdot \frac{V}{C}}{1 - \frac{V}{C}} \right) \quad \text{for } V < C \quad (3)$$

where the variables are consistent with Equations (1) and (2), and J_d is the delay parameter.

The Davidson Function gained popularity over its ability to accommodate different traffic conditions and environments (Mtoi and Moses 2014). However, the function is unable to express travel time for traffic conditions where the traffic volume exceeds the link capacity. For $V > C$, $1 - V/C < 0$, the travel time (t) for the link then decreases as traffic volume increases, which contradicts the fundamental speed-flow relationship.

2.2. Capacity models

The HCM defines capacity as the maximum amount of flow that can reasonably be expected to traverse the cross-section of a road segment. Capacity is an essential parameter in traffic state analysis, evident in its frequent occurrence in the strategic modelling VDFs. Methods in determining capacity include:

- Selected Maxima Method: states that the maximum observed flow over a period is considered as the capacity (Dervisoglu et al. 2009). This approach assumes that the actual road capacity is rarely observed due to the presence of external factors such as driver behaviour, weather conditions and other factors that prevent idealised traffic performance.
- Fundamental Diagram Method: uses speed, flow, and density data to construct diagrams that allow capacity to be observed (Rakha and Crowther 2002). Mathematical models such as Greenshield's

and Van Aerde's can be used to fit the plotted data, with the capacity being the maximum turning point of the fitted curve.

- The Product Limit Method: was initially proposed by Kaplan and Meier in 1958 (Kaplan and Meier 1958), considers a traffic breakdown as a failure event. When a sudden drop in traffic flow speed arises due to traffic demand exceeding capacity, the Product Limit Method can be used to estimate capacity based on flow observations made over the observation period.

2.3. Macroscopic modelling of CAVs

Many studies have investigated the impact of CAVs on road capacity and demonstrated that capacity increases with CAV penetration rate (CPR) (Ahmed, Dey, and Fries 2019; Ye and Yamamoto 2018; Hussain et al. 2016; Van Den Berg and Verhoef 2016; Talebpour and Mahmassani 2016 Kesting et al. 2008). There have been new contributions to the literature with alternate ways of modelling CAVs. Analytical models have been proposed to emulate the performance of a network with autonomous agents. A multiclass cell transmission model was developed to model dynamic traffic assignment (DTA) for shared road scenarios with mixed fleets of vehicles (Levin and Boyles 2016), a car following model was then developed based on driver reaction time to estimate link capacity and backwards wave speed. Capacity formulations that consider CPR, lane policies and micro/mesoscopic characteristics of vehicles have been proposed to study how the macroscopic capacity in equilibrium traffic changes with the introduction of Autonomous Vehicles (Chen et al. 2017). Both studies show consistent observations that traffic capacity increases with CPR. However, an analytical stochastic formulation which used a Markov Chain Model to describe the vehicle type distribution along the mixed fleet, demonstrated the influence of CAV platooning pattern on the spatial distribution of different headway. The study showed the necessity to consider the joint effect of CPR and CAV platooning on traffic capacity, and identified necessary conditions for the mixed traffic capacity to increase with CPR and platooning intensity (Ghiasi et al. 2017).

Based on the literature review, many studies use capacity as an indicator to evaluate the effect of CPR on traffic networks. As CPR increases, average headway decreases and effectively increases throughput. The findings in these studies are critical as they show how vehicular interactions impact the overall network performance. However, it is important to assess whether the currently used fundamental relationship between capacity and travel time still holds as the fleet transitions to CAVs. While many have proposed models and techniques for the macroscopic modelling of mixed fleets, there's limited understanding on whether a 60% saturated network with CAVs has the same travel time as an equally saturated network with HVs only. None of the studies have attempted to verify the applicability of existing methods, nor has an investigation been conducted into the effectiveness of adding a correction term to existing VDFs that more accurately reflects CAVs and mixed fleets.

3. Experimentation framework

This section is subdivided into three subsections. The first outlines the experimentation methodology, the second explains the CAV emulation algorithm, and the third explains the process for synthesising data using the case study.

3.1. Experimentation methodology

The experiment is structured as follows, and the process is outlined in the dataflow diagram provided in Figure 3:

- Establish Model Stability: Stability of the modelling environments must first be proven, to provide validity to the data they synthesise. Model stability is demonstrated in Section 3.3.1.

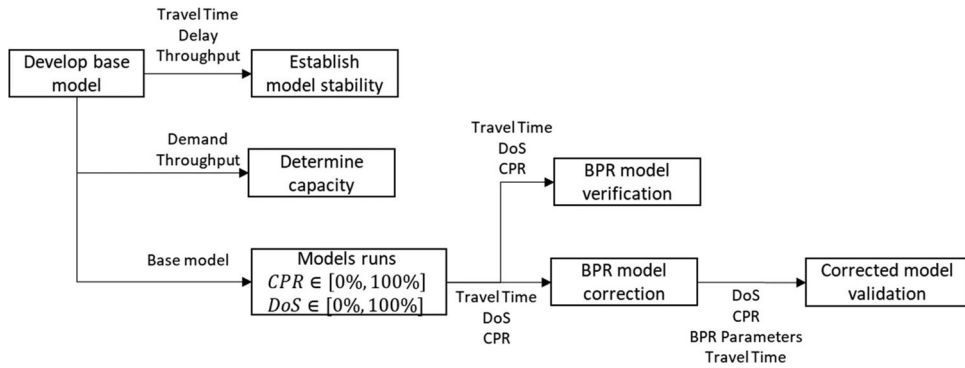


Figure 3. Dataflow diagram representing the movement of information through this study.

- Determine Environment Capacity: The capacity for each modelling environment in 20% increments of CAVs is calculated using the methodology outlined in Section 3.3.2.
- Verify BPR Performance: Synthetic data is generated for the modelling environment in 20% CPR increments and 10% DoS increments. By comparing the synthetic data with the predictions made by the BPR function, the appropriateness of its use with CAVs and mixed fleets can be determined.
- BPR Model Correction: If it is found that the BPR function does not appropriately reflect link delay for CAVs and mixed fleets, then a range of correction techniques are attempted, using the synthetic data as a means of calibration.
- Corrected Model Validation: The corrected model is then validated by comparing its predictive qualities against the BPR function in a new set of data.

3.2. CAV emulation algorithm

The CAV emulation algorithm underpins the results derived from microsimulation modelling, and so forms a critical component in the methodology of this study. For this reason, the algorithm used to emulate CAV behaviour must be rigorously critiqued and scrutinised. The algorithm is explained in detail in (Virdi et al. 2019), and has further been applied in (Virdi et al. 2019; Sinha et al. 2020a; Sinha et al. 2020b). We direct the reader to these publications for an in-depth explanation of the algorithm. The remainder of this section provides an overview of its operations in emulating CAV behaviour.

The CAV emulation algorithm dynamically considers the kinematic and spatial constraints imposed by primary and secondary lead and following vehicles. Primary and secondary leaders are assigned in response to the current environment and future intentions of the vehicle. Consider a vehicle that intends to change lanes; the primary leader and follower are the vehicles in the current lane, and the secondary leader and follower are those in the target lane. Similarly, for the vehicle that is facilitating a lane change, the primary leader is the preceding vehicle in the current lane and the secondary leader is the lane-changing vehicle. Refer to Figure 4 for a diagrammatic representation.

The purpose of dynamically assigning multiple leaders and followers is two-fold. Firstly, this approach maintains safety. Vehicles forcefully comply with their immediate car-following circumstances and react to the future intentions of itself and surrounding vehicles, reducing the possibility of sudden vehicle movements violating minimum car-following requirements. Secondly, this approach allows for mandating cooperation. Vehicles leverage vehicle-to-vehicle communication, making them aware of the future intentions of surrounding vehicles. This information then gives way to mandating cooperation and the creation of appropriate gaps, further reducing the likelihood of conflicts and imprudent lane-changing during network operation. The car-following model itself, which forms a

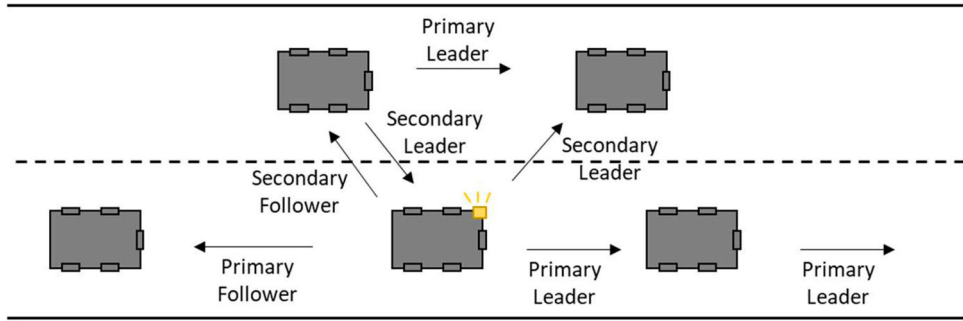


Figure 4. Diagrammatic representation of primary and secondary leaders and followers.

small part of the overall emulation framework, is an adaptation of the Van Arem et al., car-following model (Van Arem, Van Driel, and Visser 2006) and is presented in the following equation:

$$a_n(t) = k_a a_{n-1}(t - \tau) + k_v(v_{n-1}(t - \tau) - v_n(t - \tau)) + k_d(s_n(t - \tau) - s_{\text{ref}}) \quad (4)$$

where, $v_n(t)$ is the velocity of vehicle n at time t , τ is the simulation time step, s_n is the spacing between the ego and lead vehicle, s_{ref} is the minimum permitted following distance, and k_a , k_v and k_d are calibration parameters. The calibration parameters adjust the influence of the lead vehicle's behaviour on the ego vehicle. k_a , k_v and k_d do this for acceleration, velocity and headway, respectively.

Platoon members are directly linked to the actions of their immediate leaders, mimicking their actions with one time-increment delay. This control protocol results in the agency being removed from platoon followers, and the car-following model being more relevant to platoon leaders. Vehicle platooning and the coupling of a follower to its leader is calculated differently depending on which of the four regions its headway to the leader falls in. The four regions are termed stop, critical, approach, and greater than approach. The size of the region is governed by kinematic parameters such as the travel speed, maximum speed limit, maximum acceptable acceleration, maximum comfortable jerk, and maximum permitted deceleration. For a detailed mathematical definition and qualitative description of these regions, we refer the reader to (Virdi 2020). A brief definition follows;

- Greater than Approach Region: if the vehicles headway is greater than the approach distance, then a vehicle is able to evaluate the performance of the adjacent lane and decouple from its leader freely.
- Approach Region: in this region, the factors that prevent vehicles from decoupling include upcoming obstructions in trajectory such as a slowing or stopped vehicle or permanent fixed object. In this case, the vehicle is unable to decouple until the obstacle has passed.
- Critical Region: in this region, decoupling has the same condition as above, with the additional criteria that the follower surpasses the safety criteria used to define appropriate car following.
- Stop Region: if a vehicle's headway to its leader falls within the stop region, then minimum following conditions of safety and distance have been violated, and vehicles are unable to decouple.

The following are a range of use cases, where the behaviour of the algorithm is explained.

Example 3.1: The vehicle elects to remain in the current lane.

If the vehicle is a platoon follower, then the primary leader and follower are the vehicles directly adjacent in the current lane. Equation (4) is used to maintain a safe headway by ensuring that speed and spacing are not violated. Alternatively, the platoon leader has no preceding vehicle and so $a_{n-1} = 0$, the acceleration becomes governed by the parameter k_v and the difference between current and desired limit.



Figure 5. A schematic of the environment used for this study.

Example 3.2: The vehicle intends to change lanes.

The primary leader is the immediate leader of the current lane, and the secondary leader is the leader of the target lane. Both leaders impose safety constraints upon the current vehicle, as such the stricter value of the two is implemented. The acceleration of the current vehicle is calculated by equating the preceding vehicle behaviour i.e. a_{n-1}, v_{n-1} in Equation (4) to the behaviour of the primary or secondary leader. The ego vehicle's acceleration then subtends to the lowest value, ensuring cooperation with the vehicles in the target lane and maintaining safety with the vehicles in the current lane. The sudden change in acceleration is limited to 0.5 m/s^3 .

Example 3.3: The adjacent vehicle intents to change lanes.

The lane-changing vehicle becomes the secondary leader of the current vehicle, and the primary leader is the immediate leader in the current lane. This condition reflects the cooperative nature of CAVs, as the current vehicle will facilitate lane change for the secondary leader by adjusting acceleration and providing adequate headway. The sudden change in acceleration is limited to 0.5 m/s^3 .

3.3. Case study

This investigation begins with the development of a testbed. The details of the environment and proof of its stability is provided in Section 3.3.1. Once stability is established, capacity must be determined for each CPR. The literature review in Section 2.2 provided a range of methods through which to calculate capacity, however, none were considered appropriate. The methodology for calculating corridor capacity is provided in Section 3.3.2.

3.3.1. Microsimulation environments

Three testbeds are used in this study to generate data. Each testbed is a hypothetical 'Type A Weaving' motorway section consisting of three sets of on-ramps and off-ramps. Figure 5 displays a single section; the full modelling environment consists of three of these joined consecutively.

Type A weaving manoeuvre requires vehicles in both directions to make one lane change to successfully complete a weaving action (Highway Capacity Manual 2000). Four traffic movements form the weaving environment;

- On-Ramp to Off-Ramp (Through movement)
- On-Ramp to Mainline (Weaving)
- Mainline to Off-Ramp (Weaving)
- Mainline to Mainline (Through movement)

The three testbeds differ in weaving area length, speed limit, and weaving proportion. Refer to Table 1 for the differences between the three testbeds.

The parameters between the different testbeds were designed to replicate extreme weaving conditions that are observed in traffic network. The distance between onramps and offramps is inspired by the Western Distributor as shown in Figure 6, located in the Sydney motorway network.

This section of the network has approximately 6 ramps along a 1.8 km section (i.e. approximately 300 m apart). The weaving proportions were identified using the Westlink M7 publicly available ramp-to-ramp motorway data (Transurban 2020). This dataset was used to identify tentative high, medium,

Table 1. The weaving length, speed limit and weaving proportion used to differentiate the three testbeds.

		Segment 1	Segment 2	Segment 3
Speed Limit		90 km/hr	80 km/hr	100 km/hr
Weaving length	Testbed 1	200 m	250 m	300 m
	Testbed 2	250 m	250 m	250 m
	Testbed 3	300 m	250 m	200 m
Weaving proportion	Testbed 1	15.00%	22.77%	33.01%
	Testbed 2	19.39%	22.34%	30.77%
	Testbed 3	23.47%	22.68%	19.10%

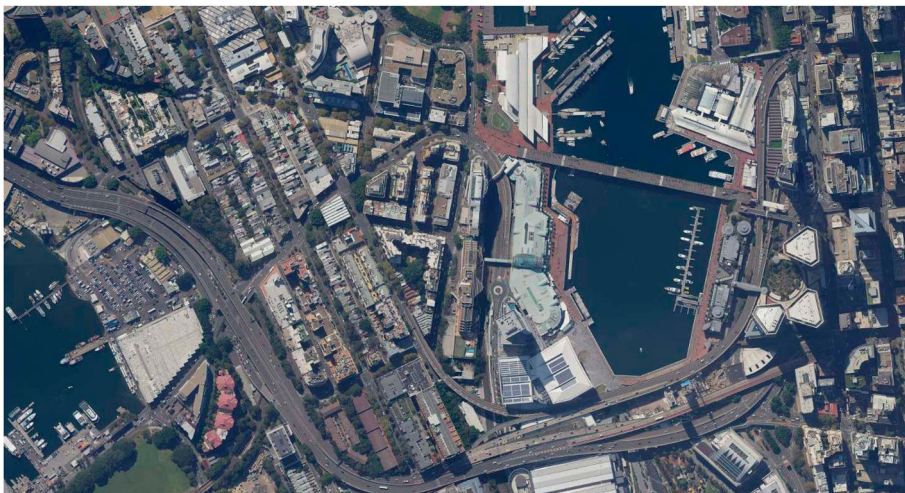


Figure 6. Western distributor, Sydney, Australia. Source: SIX Maps (2021).

and low values of weaving proportions near motorway ramps. The speed limits used correspond with this that are typical of high-capacity arterial (80 km/h), freeway (90 km/h), and motorways (100 km/h) in Sydney.

Each on-ramp has a form of ramp metering to ensure that weaving vehicles do not cause a choke point to arise and artificially restrict flow. The ramp metering operates by holding vehicles on the ramp until the adjacent mainline average travel speed returns to a minimum of 50 km/h. CAV behaviour is controlled by the framework presented in Section 3.2, and human behaviour is controlled by the microsimulator (VISSIM) using the Wiedemann 99 Model (PTV Group 2016).

The naming convention for the zones in the base origin-destination (OD) matrix is as follows. The mainline is the main motorway movement, with vehicles travelling from East ('Mainline On') to West ('Mainline Off'). The ramps are numbered sequentially in order of appearance, starting with 1 in the East and 3 in the West. 'On' and 'Off' ramps have the appropriate suffix appended to their name. So a vehicle travelling from the mainline to the third off-ramp would be labelled as 'Mainline On to Ramp 3 Off'. Using this naming convention, Table 2 provides the base origin-destination matrix for each of the testbeds. To moderate demand in the network, the base case matrices are multiplied by an integer scaling factor.

The number of weaving vehicles in the first weaving section is the summation of vehicles travelling from 'Mainline On' to 'Ramp 1 off' and vehicles travelling from 'Ramp 1 On' to every destination bar 'Ramp 1 Off'. This amounts to a weaving vehicle proportion of 15% in the first Section, 20% in the second Section and 33% in the final Section.

Table 2. The base origin-destination matrices used for each testbed in this study.

O\D	Ramp 1 off	Ramp 2 off	Ramp 3 off	Mainline off	Total
<i>Testbed 1</i>					
Mainline On	6	12	13	57	88
Ramp 1 On	3	2	3	4	12
Ramp 2 On		1	3	6	10
Ramp 3 On			2	15	17
Total	9	15	21	82	127
<i>Testbed 2</i>					
Mainline On	10	11	13	52	86
Ramp 1 On	3	2	3	4	12
Ramp 2 On		1	3	5	9
Ramp 3 On			2	9	11
Total	13	14	21	70	118
<i>Testbed 3</i>					
Mainline On	10	11	6	55	82
Ramp 1 On	3	2	3	8	16
Ramp 2 On		3	3	6	12
Ramp 3 On			3	5	8
Total	13	16	15	74	118

Table 3. Network statistics used to establish model stability.

	Average delay	Average speed	Average travel distance	Average travel time
Testbed 1	20.12%	5.18%	0.25%	5.43%
Testbed 2	14.87%	2.80%	0.30%	2.95%
Testbed 3	13.93%	7.37%	0.88%	6.91%

Each value is the proportion of the standard deviation of all runs, to the median value. Fifty iterations for each testbed was used.

Model stability is established by running 50 iterations of each testbed using 0% CAVs and a network demand at capacity. The standard deviation of the key network metrics (average delay, average travel time, average travel distance and average speed) were calculated as a proportion of the mean value. The network results of the stability analysis are provided in Table 3. The average delay has a higher deviation compared to the other metrics, which is an expected outcome for environments operating near capacity. The other metrics show little variance compared to their mean values.

Each iteration uses a warm-up period of 30 min, where the network is loaded with 80% of the peak hour demand. The warm-up period is then followed by a peak modelling period of 1 h, which is used for network evaluation.

3.3.2. Capacity calculation

Capacity plays a critical role in the BPR function. If the capacity of an environment is not known accurately, then the use of an approximation in the BPR function would compound error upon error, potentially leading to a disingenuously inaccurate result. For this reason, extensive efforts have been taken in determining the corridor capacity. While many of the approaches presented in Section 2.2 were explored to determine capacity here, they were not deemed appropriate for this study. Those approaches either required an unreasonably intimate knowledge of the corridor and specific driving behaviour, or they provided approximations, the accuracy of which would be difficult to verify.

This study used a modified version of the Selected Maxima Method. Since the localised factors that affect capacity in this corridor were unknown, the network was incrementally loaded, and throughput was observed. Data were collected on each of the three off-ramps, as well as the two lanes leading to the end of the model. The environment was then incrementally loaded with traffic by multiplying the base OD matrix by a factor that started at 1 and was gradually increased by 1. The total throughput

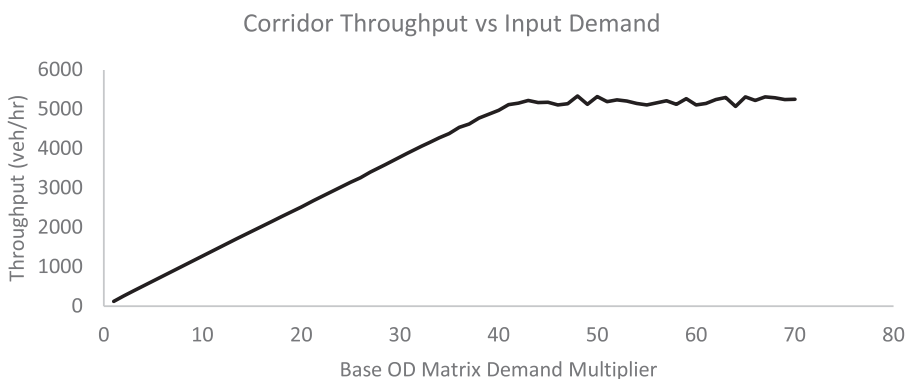


Figure 7. Corridor throughput plotted against corridor demand, used to calculate the modelling environment capacity.

Table 4. The quantitative values used to generate Figure 5, also showing the rate of change for demand and throughput. This table is also used to inform capacity.

Demand Multiplier	Total Through	Δ Demand	Δ Through	$\frac{\Delta \text{ Demand}}{\Delta \text{ Through}}$	Running Average
37	4621	3%	2%	67%	92%
38	4776	3%	3%	124%	105%
39	4870	3%	2%	75%	89%
40	4974	3%	2%	83%	94%
41	5114	2%	3%	113%	90%
42	5153	2%	1%	31%	76%
43	5225	2%	1%	59%	68%
44	5170	2%	-1%	-45%	15%
45	5174	2%	0%	3%	6%
46	5109	2%	-1%	-57%	-33%
47	5135	2%	1%	23%	-10%
48	5335	2%	4%	183%	50%

of the network is calculated by summing the volume measured at each of the detectors. An example plot of total throughput against the demand multiplier is provided in Figure 7.

Incrementally loading the corridor reduces the complexity in identifying its capacity. Referring to Figure 7, the capacity is defined as the point where an appreciable increase in corridor demand does not lead to an appreciable increase in throughput, when the gradient of the plot approaches 0. This method still contains ambiguity in determining capacity, especially for a random seeds numbers or a CPR that do not exhibit a clear relationship between the corridor throughput and loaded demand. Consider the additional information provided in Table 4, which provides the percentage change in demand, the percentage change in throughput, a ratio of the two metrics, and a 3-value running average.

In Table 4, the pale yellow colour depicts the demand multipliers that result in an undersaturated corridor, the darker orange colour depicts the oversaturated environment, and the unique orange colour results in the corridor reaching capacity. The criteria used for this evaluation is as follows. When $\frac{\Delta \text{Demand}}{\Delta \text{Through}}$ is near 100%, it indicates that the incremental demand loaded to the network was able also to reach the detectors at the exit points, and hence the network is still performing in an unhindered state below capacity. As this network is further loaded, this ratio drops which indicates proportionally less throughput than in the previous case.

Table 5. Capacity for each testbed and each CAV penetration.

	CAV penetration rate (%)										
	0	10	20	30	40	50	60	70	80	90	100
Testbed 1	44	46	49	53	55	58	63	68	73	80	82
Testbed 2	49	51	52	55	59	65	68	72	75	80	84
Testbed 3	47	49	52	55	59	64	69	74	77	83	85

Table 6. Change in capacity for each testbed and each CAV penetration rate, relative to the base case 0% CAV scenario.

	CAV penetration rate (%)										
	0	10	20	30	40	50	60	70	80	90	100
Testbed 1	5%	11%	20%	25%	32%	43%	55%	66%	82%	86%	
Testbed 2	4%	6%	12%	20%	33%	39%	47%	53%	63%	71%	
Testbed 3	4%	11%	17%	26%	36%	47%	57%	64%	77%	81%	

Setting a threshold for this ratio is not adequate for defining capacity. Due to the inherent stochasticity of microsimulation modelling, a particular run may show a decrease in throughput while the next may show an increase that more than sufficiently compensates. For this specific reason, an average of the previous 3 results is used, dubbed as the ‘running average’ in Table 4. While placing a threshold on the running average provided substantially more representative calculations for capacity, it also was limited in its usefulness when consecutive runs tend to oscillate around a value. In rare cases where the oscillation occurred, manual selection of the capacity multiplier was made.

4. Results

This Section provides the results for the experimentation. The results are segregated into the subsections mentioned in Section 3.1. Note that the demand values in this Section are a multiplication factor for the base case matrices provided in Table 2.

4.1. Testbed capacity

Capacity for each testbed and each CAV penetration was found by incrementally loading the network with demand and using the process identified in Section 5.2. This capacity value is not reliable, as random seeds and natural microsimulation stochasticity render any one modelling result insignificant unless it is benchmarked against other results. For this reason, 300 iterations of the of each testbed for each CAV penetration rate are conducted, where the demand was randomly generated for $\text{DoS} \in [0, 1.1]$ and random seed (RS) was randomly generated for $\text{RS} \in [1, 99999]$. Figure 8 provides the throughput recorded for each iteration.

Figure 8 demonstrates that while each testbed is undersaturated, an increase in demand leads to an identical rise in throughput. For each CPR, the environment reaches a point where the Demand vs Throughput plot becomes horizontal and additional demand does not increase throughput further. This point is defined as capacity. Table 5 provides the quantitative value for capacity, for each CPR and each testbed.

The values in Table 5 are used to define the different DoS scenarios. The increase in capacity relative to the 0% CAV case for each testbed is provided in Table 6.

4.2. Verify BPR model performance

Verification of the BPR model requires synthetic data. Synthetic data were generated for all three testbeds, CAVs $\in [10\%, 100\%]$ in 10% increments, $\text{DoS} \in [10\%, 100\%]$ in 10% increments, and 20

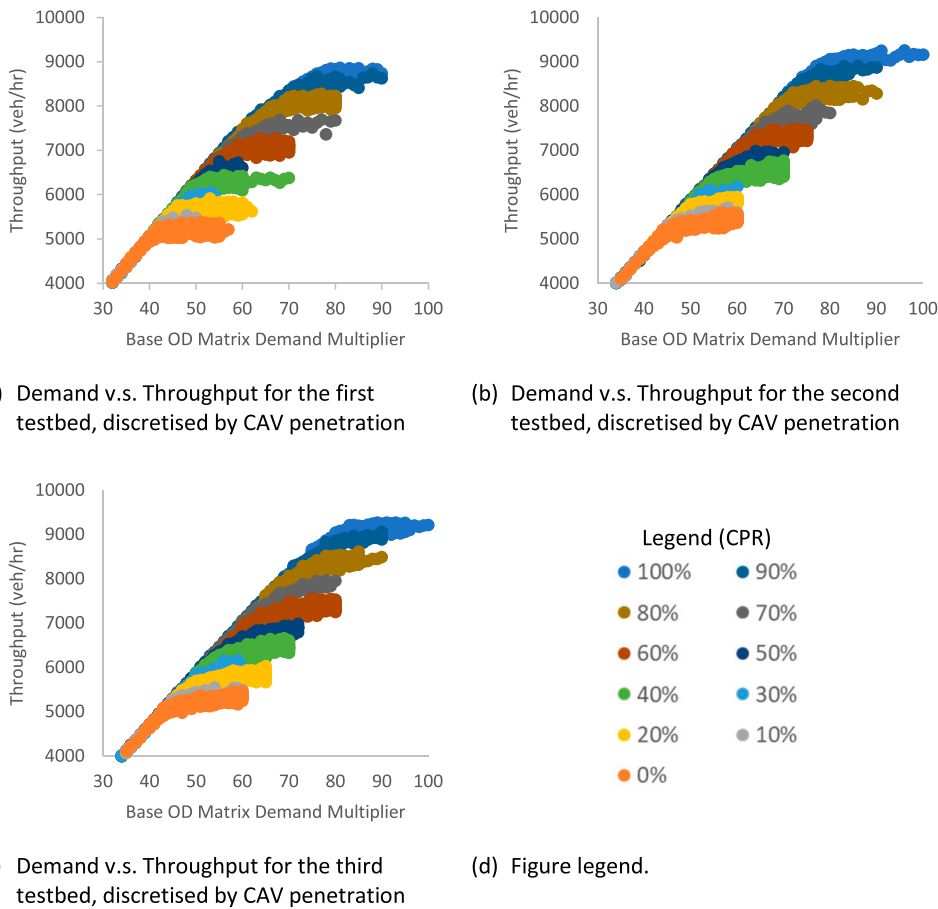


Figure 8. Plotting throughput vs. demand, to determine the environment capacity for different CAV penetrations. The capacity is defined as the inflection point where an increase does not lead to an appreciable increase in throughput.

randomly generated iterations for each case. This structure amounts to a total of 6,600 iterations of the modelling. The synthetic data was then aggregated into two groups, 30% reserved for the VDF model evaluation and recalibration, and the remaining 70% reserved for VDF model recalibration if it is warranted.

Table 7 below indicates the average travel time through the microsimulation environment for different CAV penetration rates and DoS rates. This table shows that travel time increases with travel demand, as the network reacts rationally to growing levels of congestion.

Table 8 demonstrates the difference in the travel time calculated through the synthetic data, and the travel times predicted by the BPR function. For the BPR function to be used appropriately, its parameters must be calibrated for each use case. The BPR α and β values that minimised error between the synthetic data and the prediction made by the BPR function were used ($\alpha = 1.0122$ and $\beta = 4.1856$). Deviations in travel time predictions are as follows.

Table 8 shows that despite the BPR parameters being calibrated to minimise error, the BPR tends to incorrectly predict travel time when DoS increases and when CPR increases. The RMSE for the BPR function is 11.56, 9.68 and 7.95, for the three testbeds respectively. Decreasing the weaving proportion from Testbed 1 to Testbed 3 reduced the error of the BPR corridor travel time predictions. To contextualise this error in travel time estimation, consider the scenario that generated the highest error value of 48 s/veh. This scenario had a demand of 9912 vehicles. This implies a total system delay of 476,000 s

Table 7. Average travel time (sec) for each CPR, DoS and testbed, averaged for a randomly selected 30% of the synthetic data.

Testbed 1 - Average Travel Time (sec)										
CPR\DoS	10%	20%	30%	40%	50%	60%	70%	80%	90%	100%
0%	78	79	79	80	80	82	86	95	124	214
10%	78	79	79	80	81	83	87	98	134	212
20%	78	79	79	80	81	83	90	99	137	201
30%	79	79	80	80	82	85	93	110	156	211
40%	78	79	80	80	82	84	93	101	141	174
50%	79	79	80	81	83	86	93	109	142	177
60%	79	80	81	81	84	85	98	101	144	149
70%	79	80	81	82	84	89	101	118	139	171
80%	79	80	81	82	86	88	99	106	141	141
90%	80	81	82	84	87	95	107	123	139	143
100%	80	81	82	84	89	93	111	114	128	131
Testbed 2 - Average Travel Time (sec)										
CPR\DoS	10%	20%	30%	40%	50%	60%	70%	80%	90%	100%
0%	88	88	89	90	91	92	95	101	144	162
10%	88	88	89	90	91	93	96	107	144	169
20%	88	88	89	90	91	93	96	102	134	157
30%	88	89	90	91	92	94	97	109	137	166
40%	88	89	90	91	92	93	101	105	145	158
50%	89	89	90	91	93	96	103	119	148	166
60%	89	90	91	91	93	96	105	111	142	156
70%	89	90	91	92	94	97	104	115	139	156
80%	89	90	92	92	95	97	105	110	127	139
90%	90	91	92	93	95	98	105	112	126	137
100%	90	91	92	93	95	96	103	106	123	127
Testbed 3 - Average Travel Time (sec)										
CPR\DoS	10%	20%	30%	40%	50%	60%	70%	80%	90%	100%
0%	70	71	71	72	74	75	80	88	116	162
10%	70	71	72	73	74	77	81	94	135	168
20%	71	71	72	73	74	77	83	93	130	150
30%	71	71	72	73	75	78	86	100	134	158
40%	71	72	72	73	76	78	89	95	139	144
50%	71	72	73	74	77	81	92	108	135	158
60%	71	72	73	74	78	79	94	99	134	134
70%	72	73	74	76	79	85	95	110	128	137
80%	72	73	74	76	79	82	93	99	120	125
90%	72	74	75	77	81	86	94	105	116	122
100%	73	74	76	78	82	85	93	98	112	116

in the 1 h modelling period for this 3-link corridor. Extrapolating to a citywide network would result in substantially poor modelling results. For this reason, recalibrating the BPR function parameters to predict delay in mixed-fleet environments is attempted in the remainder of this paper.

4.3. BPR model recalibration

The BPR function has no capabilities to cater to CAV penetration. This section starts by proposing a unique α and β for each CAV penetration, for each testbed. The unique α and β parameters were

Table 8. Difference in the average travel time predicted by the BPR function, and the average travel time found using the synthetic data.

Testbed 1 – Difference between Synthetic and BPR Travel Time (sec)										
CPR\DoS	10%	20%	30%	40%	50%	60%	70%	80%	90%	100%
0%	-1	-1	-1	0	1	5	9	14	4	-58
10%	-1	-1	-1	-1	1	4	8	11	-6	-56
20%	-1	-1	-1	-1	0	3	5	9	-9	-45
30%	-1	-1	-2	-1	0	2	2	-1	-28	-55
40%	-1	-2	-2	-1	-1	2	2	7	-13	-18
50%	-1	-2	-2	-2	-1	1	2	-1	-14	-21
60%	-1	-2	-3	-2	-2	1	-3	7	-16	6
70%	-2	-3	-3	-3	-3	-2	-5	-10	-11	-15
80%	-2	-3	-3	-3	-4	-1	-4	2	-13	15
90%	-2	-3	-4	-5	-6	-8	-12	-15	-12	12
100%	-2	-4	-4	-4	-7	-6	-16	-6	0	25
Testbed 2 – Difference between Synthetic and BPR Travel Time (sec)										
CPR\DoS	10%	20%	30%	40%	50%	60%	70%	80%	90%	100%
0%	-1	-1	-2	-1	1	5	11	20	0	13
10%	-1	-1	-2	-1	1	4	11	15	-1	6
20%	-1	-1	-2	-1	1	5	11	19	9	18
30%	-1	-2	-2	-2	0	3	9	13	7	9
40%	-1	-2	-2	-2	0	4	6	16	-1	17
50%	-2	-2	-3	-2	-1	1	4	3	-4	9
60%	-2	-3	-3	-3	-2	2	1	10	1	18
70%	-2	-3	-4	-3	-2	0	3	6	4	19
80%	-2	-3	-4	-4	-3	1	2	12	16	36
90%	-3	-4	-5	-4	-3	-1	2	9	18	38
100%	-3	-4	-5	-4	-3	1	4	15	21	48
Testbed 3 – Difference between Synthetic and BPR Travel Time (sec)										
CPR\DoS	10%	20%	30%	40%	50%	60%	70%	80%	90%	100%
0%	-1	-1	-1	-1	0	4	6	9	0	-21
10%	-1	-1	-1	-1	0	1	5	4	-19	-27
20%	-1	-1	-1	-1	0	2	3	5	-15	-10
30%	-1	-1	-2	-1	-1	0	0	-2	-18	-17
40%	-1	-2	-2	-2	-2	0	-3	3	-24	-3
50%	-1	-2	-2	-3	-3	-3	-6	-10	-19	-17
60%	-1	-2	-3	-3	-4	-1	-8	-1	-18	7
70%	-2	-3	-3	-4	-5	-6	-9	-13	-12	3
80%	-2	-3	-4	-4	-5	-4	-7	-1	-5	16
90%	-2	-3	-5	-6	-7	-8	-8	-7	-1	19
100%	-3	-4	-5	-6	-8	-7	-7	0	3	25

optimised to minimise the delay for each CAV penetration. The resulting optimised parameter are plotted in Figure 9.

The variance between optimised values from the different testbeds is low. Using these data points, a linear model is fitted to the average value of the three testbeds. The linear best fit model for the α and β parameter is provided in Figure 10.

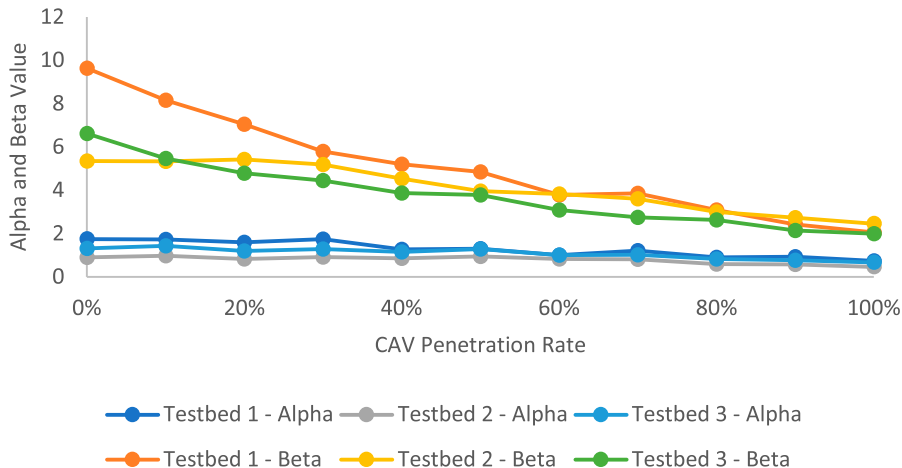


Figure 9. The optimal α and β values for each CPR and testbed.

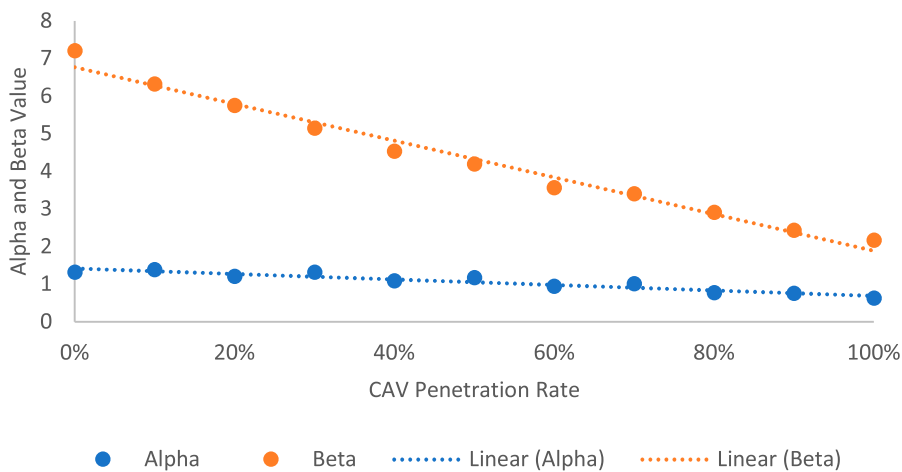


Figure 10. The linear models fitted to α and β parameters.

The r^2 value describing the goodness of fit of the linear model is 0.9013 and 0.9821 for the α and β parameters respectively. The calibrated linear models for both parameters is provided in Equation (5).

$$\begin{aligned} \alpha &= -0.7302 \times \text{CPR} + 1.4193 \\ \beta &= -4.8811 \times \text{CPR} + 6.7691 \\ \text{Where, } \text{CPR} &\in [0, 1] \end{aligned} \quad (5)$$

4.4. Corrected model validation

The recalibrated BPR parameters were used to develop an α and β model with respect to CPR. The predictive qualities of the recalibrated model are evaluated by using the remaining 70% of the synthetic data. Provided in Table 9 is the difference in synthetically generated travel time and that predicted by the recalibrated model, similar to Table 8 developed for the BPR model.

To directly compare the performance of the original BPR model to the recalibrated variant, the ratio of the RMSE of both models is used for each scenario. In Table 10 below, a value between 0 and 1 in

Table 9. Difference in the average travel time predicted by the calibrated model, and the average travel time found using the synthetic data.

Testbed 1 – Difference between Synthetic and Recalibrated BPR Travel Time (sec)										
CPR\DoS	10%	20%	30%	40%	50%	60%	70%	80%	90%	100%
0%	-1	-1	-1	-2	-2	-1	1	7	7	-26
10%	-1	-1	-2	-2	-2	-1	1	5	-2	-30
20%	-1	-1	-2	-2	-2	-1	0	5	-6	-24
30%	-1	-1	-2	-2	-2	-1	-2	-4	-26	-40
40%	-1	-2	-2	-2	-2	1	0	6	-11	-9
50%	-1	-2	-2	-2	-1	1	2	-1	-13	-18
60%	-1	-2	-2	-1	-1	3	-1	8	-16	4
70%	-2	-2	-2	-1	0	1	-2	-8	-12	-23
80%	-2	-2	-2	0	0	4	1	5	-15	1
90%	-2	-2	-1	0	1	0	-4	-11	-16	-7
100%	-2	-1	1	3	3	5	-6	-2	-7	0
Testbed 2 – Difference between Synthetic and Recalibrated BPR Travel Time (sec)										
CPR\DoS	10%	20%	30%	40%	50%	60%	70%	80%	90%	100%
0%	-1	-1	-2	-3	-3	-1	2	13	3	49
10%	-1	-2	-2	-3	-3	-1	3	9	3	35
20%	-1	-1	-2	-3	-2	0	5	15	13	40
30%	-1	-2	-3	-3	-2	0	5	10	10	26
40%	-1	-2	-3	-2	-2	2	4	15	1	27
50%	-2	-2	-3	-3	-2	1	3	3	-3	13
60%	-2	-3	-3	-2	-1	3	3	12	2	16
70%	-2	-3	-3	-2	0	4	7	9	3	10
80%	-2	-3	-2	0	2	7	8	15	13	21
90%	-3	-3	-1	2	5	8	11	13	13	16
100%	-2	-2	1	4	8	13	15	20	13	20
Testbed 3 – Difference between Synthetic and Recalibrated BPR Travel Time (sec)										
CPR\DoS	10%	20%	30%	40%	50%	60%	70%	80%	90%	100%
0%	-1	-1	-1	-2	-3	-2	-1	3	3	8
10%	-1	-1	-2	-2	-3	-3	-1	0	-16	-4
20%	-1	-1	-2	-2	-2	-2	-1	2	-12	9
30%	-1	-1	-2	-2	-3	-2	-3	-4	-16	-4
40%	-1	-2	-2	-2	-3	-1	-5	2	-22	5
50%	-1	-2	-3	-3	-3	-3	-6	-10	-18	-14
60%	-1	-2	-3	-2	-3	0	-6	0	-18	5
70%	-2	-2	-3	-3	-2	-3	-6	-10	-13	-4
80%	-2	-3	-3	-2	-1	1	-2	2	-7	3
90%	-2	-2	-2	-1	0	-1	-1	-4	-5	2
100%	-2	-2	-1	1	1	3	1	4	-3	2

green indicates that the recalibrated model outperformed the original BPR function. A value greater than 1 in red indicates the opposite, that the BPR outperformed the recalibrated function.

Through visual inspection of Table 10 above, it is clear that there are specific points where the recalibrated model performs significantly worse than the original BPR model. However, the overarching distribution of green indicates that the model as a whole operates better. Visual inspection alone is insufficient to conclude, a qualitative assessment follows.

At face value, Table 10 provides a range of instances indicating that the original BPR outperforms the modified function. However, these instances are predominately concentrated at DoS values of less

Table 10. A direct comparison of the BPR function vs. its recalibrated variant. A green value indicates the recalibrated model outperformed the original BPR, with a red value indicating the opposite.

Testbed 1 – Accuracy in travel time prediction – BPR v.s. Recalibrated										
CPR\DoS	10%	20%	30%	40%	50%	60%	70%	80%	90%	100%
0%	1.01	1.11	1.49	3.83	1.70	0.43	0.17	0.53	2.72	0.29
10%	1.01	1.09	1.42	2.84	2.16	0.32	0.24	0.61	2.41	0.50
20%	1.01	1.08	1.30	2.42	5.32	0.25	0.03	0.61	0.80	0.47
30%	1.01	1.05	1.22	1.71	7.87	0.68	0.48	2.90	0.91	0.69
40%	1.00	1.04	1.13	1.49	3.52	0.31	0.06	0.89	0.86	0.37
50%	1.00	1.01	1.03	1.08	1.32	0.49	0.84	0.52	0.89	0.89
60%	1.00	0.97	0.91	0.71	0.50	1.88	0.12	1.20	0.98	0.21
70%	0.98	0.90	0.75	0.49	0.17	0.00	0.05	0.72	1.07	1.83
80%	0.96	0.79	0.54	0.03	0.21	3.87	0.01	2.79	1.26	0.06
90%	0.89	0.65	0.28	0.09	0.25	0.02	0.34	0.72	1.36	0.87
100%	0.72	0.32	0.13	0.72	0.46	0.69	0.33	0.30	9.05	0.01
Testbed 2 – Accuracy in travel time prediction – BPR v.s. Recalibrated										
CPR\DoS	10%	20%	30%	40%	50%	60%	70%	80%	90%	100%
0%	1.01	1.09	1.37	2.99	3.06	0.26	0.19	0.61	1.39	4.49
10%	1.01	1.06	1.35	2.26	4.42	0.32	0.26	0.63	2.61	31.33
20%	1.01	1.06	1.25	2.15	4.45	0.01	0.44	0.79	1.32	2.45
30%	1.00	1.05	1.19	1.68	116.15	0.04	0.51	0.79	1.34	4.42
40%	1.00	1.03	1.11	1.39	5.53	0.45	0.68	0.92	1.85	1.64
50%	1.00	1.01	1.02	1.06	1.21	0.53	0.93	1.18	0.73	1.56
60%	1.00	0.97	0.92	0.77	0.35	1.86	1.57	1.17	6.16	0.83
70%	0.99	0.92	0.76	0.49	0.57	39.99	2.87	1.79	0.65	0.56
80%	0.96	0.82	0.56	0.06	1.04	9.44	3.03	1.34	0.79	0.54
90%	0.90	0.66	0.30	0.35	1.53	7.77	3.93	1.52	0.66	0.42
100%	0.75	0.35	0.13	1.02	2.68	11.09	3.86	1.32	0.65	0.43
Testbed 3 – Accuracy in travel time prediction – BPR v.s. Recalibrated										
CPR\DoS	10%	20%	30%	40%	50%	60%	70%	80%	90%	100%
0%	1.01	1.11	1.45	3.29	4.08	0.56	0.39	0.30	0.24	0.51
10%	1.01	1.08	1.38	2.41	7.51	0.82	0.26	0.14	0.71	0.08
20%	1.01	1.07	1.27	1.96	5.71	1.06	1.55	0.47	0.83	0.05
30%	1.01	1.05	1.19	1.52	3.21	6.09	2.57	1.92	0.88	0.45
40%	1.00	1.03	1.11	1.32	1.62	0.97	1.56	0.76	0.91	0.36
50%	1.00	1.01	1.02	1.05	1.08	1.08	1.03	0.98	0.95	0.79
60%	1.00	0.97	0.93	0.81	0.76	0.26	0.80	2.75	0.99	0.62
70%	0.99	0.92	0.81	0.65	0.49	0.50	0.61	0.84	1.07	11.83
80%	0.96	0.84	0.65	0.32	0.27	0.23	0.34	0.39	1.67	0.17
90%	0.91	0.70	0.44	0.20	0.15	0.10	0.21	0.49	2.42	0.04
100%	0.75	0.46	0.16	0.18	0.16	0.47	0.19	75.27	1.71	0.02

than 40%, where the network is well below saturation. In this region of near free-flow performance and near 0 s delay, small absolute differences between the observed travel time and estimated travel time result in large error ratios. For this reason, the slight outperformance of the recalibrated BPR by the original BPR function in this region do not provide an appropriate conclusion for or against the calibrated function.

For instances where there is a significantly better performance by the original BPR (i.e. the locations of Dark Red in Table 10), this is the result of a coincidentally near-perfect prediction by the original BPR function. Consider Testbed 2 in Table 10, the DoS = 50% and CPR = 30% scenario, the difference

between observed travel time and the travel time predicted by the recalibrated function is approximately 2 s. While the absolute difference in the prediction error is small, because the original BPR was coincidentally almost perfect in its prediction with a near-zero difference, resulting in the very large ratio of 116.15. Extremely large and extremely small values reported in Table 10 should be treated with a note of caution due to this occurrence.

To compensate for this limitation in the assessment technique, the results were also calculated at an aggregate scale where the absolute number of cases in which the calibrated function out-performed the original function, meaning the value is independent of the magnitude of the improvement. When considering the aggregated synthetic data, and applying the two BPR variants to each data point, the original model yields an RMSE of 15.16, whereas the recalibrated BPR yields an RMSE of 8.86. This change amounts to a model improvement of 42%. This improvement is comprised of 67% of the data points showing an improvement in travel time prediction, with the remaining 33% showing a worse prediction. However, the 67% could have potentially been composed of negligible improvement, while the remaining 33% showed significantly worse performance. By assessing the absolute improvement in travel time prediction, the significance of the improvement can be investigated. The average improvement of all data points is 543%. This figure indicates that the improvements in travel time prediction are 5.43 times better than any errors arising from the new BPR model. The predictive qualities of the new approach, while not flawless, far outweigh the predictive qualities of the original BPR model in a mixed fleet environment.

4.5. Commentary on the stochastic properties of platooning

A limitation of this study is in its treatment of random arrival and traffic generation. CAVs and human vehicles in this study are stochastically generated and distributed as they are loaded onto onramps and into the network. By conducting 20 simulations per scenario, with a total number of runs of 6600 in this study, we adequately account for the randomness in vehicle generation. Randomness in arrival was accounted for this way because a position on upstream intersection control was not assumed in this study. A centralised intersection controller upstream of the onramps that optimises intersection performance based on an objective function may change the arrangement of CAVs and Human vehicles arriving on the onramp. However, if upstream intersections are priority-controlled or signalised, then arrivals may continue to be random. Without clarity or assumption of the upstream intersection controller, random arrival is assumed in this study.

4.6. Commentary on the Conic and Davidson VDFs

A similar methodology was used to attempt a recalibration of both the Conical and Davidson VDFs, with neither showing positive results. This methodology was successfully applied to the BPR function due to the simple nature of the model. The α and β parameters occur in the BPR function once, making their role both tractable and relatable to real-world phenomena. Therefore, altering the model has a predictable consequence that also reflects the change observed in real-world fleet operation or in synthetic data. The Conical and Davidson function, however, have a complex relationship between the travel time prediction and their calibration parameters (refer to Equations (2) and (3)). This complex relationship results in modifications to the model, as conducted for the BPR function, having unintended consequences. The methodology used in this study for recalibrating the BPR function is not appropriate for either the Conical function or the Davidson function.

5. Discussion

The results reported in Section 4 demonstrate that the traditional BPR function performs well for under saturated conditions, but performs poorly as congestion or CAV penetration increases. When the α and β parameters are recalibrated as functions of CPR, the predictive qualities of the BPR function

improve. Before and after recalibration, the BPR function RMSE improved from 15.16 to 8.86. In 67% of cases, the recalibrated variant better predicted travel time than the traditional BPR function. Finally, of the 4620 simulation runs, forming the 70% of the dataset used for validation, the recalibrated BPR function better-predicted travel time by 5.43 times.

The implications of the results of this study is two-fold. Firstly, this study demonstrates that the BPR function can benefit from a recalibration, making its form more appropriate for use with mixed-fleets and CAVs. Secondly, this study demonstrates that for legacy purposes, the BPR function does not need to be explicitly replaced with more complicated and sophisticated models developed specifically for CAVs. The review of relevant literature demonstrated that alternative approaches for mixed-fleet and CAV VDFs relying on artificial intelligence, and machine learning requires substantial quantities of data for training and calibration purposes. Other approaches proposed in the literature are not as simple and accessible as the BPR function. For this reason, validating its continued use is critical.

There are, however, questions raised in regards to the methodology used in this study, that warrant further investigation. The original BPR function was developed by curve-fitting a model to data observed from a single motorway section in the United States. The small dataset used for calibration significantly narrows the use-cases in which the parameters recommended in the HCM are appropriate. For this reason, the HCM recommends recalibrating the BPR model parameter for each environment in which it is used. While this study used three different testbeds and a further three segments in each testbed for a total of nine weaving segments to synthesise the data, it still followed a similar methodology to that used in the development of the original BPR function. This implies that the calibration and validation synthetic data used in this study may require site-specific correction.

Additionally, this study demonstrated that the weaving proportion affected the optimal α and β parameters. Figure 9 showed that the variance in the optimum parameters is higher for low CAV penetrations (less than 20%). Therefore, it is less reliable to use a curve-fitted model to calculate the parameter for lower CAV penetration rates. Table 9 reconfirms this expectation, as travel time predictions in the low CPR and high DoS region tend to show a greater error against the observed travel time. Altering the parameters to be functions of CPR may not be enough. If the parameters also show sensitivity to vehicle weaving proportions, speed limits, weaving segment length and other factors, then also including these factors in the parameter function may yield improved results. However, each additional factor included in the assessment exponentially increases the data required and the modelling time, especially if a covariate assessment approach is used.

The CAV emulation framework used in this study and presented in Section 4 is underpinned by the critical assumption of cooperativeness. The weaving proportion of vehicles is distinct in the three adjacent weaving sections, and travel time results indicate a worsen travel time with increasing weaving proportion (refer to Table 7). This study used weaving proportions of up to 33%, which is relatively high compared to what real network experience. Had the weaving performance been lower, the recalibration and prediction efforts may have yielded further improvements than they already did. That is to say, the results of this study are a conservative estimate of the benefit derived from recalibrating the BPR function.

During the recalibration process of the BPR parameters, a linear best-fit model was used as it provided a high r^2 value for both parameters and is simple. This decision raises two key questions. The first, would an alternate model have yielded better results? The second, what are the real-world implications or justifications for using a specific model, and the value of the parameters? This study demonstrated that α and β are both inversely and linearly proportional to CPR. In the BPR function, lowering the value of β reduces the gradient of the travel time increase between a DoS of 0 and approximately 0.8, resulting in a sharper increase in travel time between DoS 0.8 and 1. Increasing the α parameter increases the magnitude of the travel time increase at a DoS of 1. Refer to Figure 2 for a diagramtic representation of these trends. To say that CAVs have an inversely linear relationship means that increasing the CAV penetration reduces the travel time impact of proportionally additional demand. The relationship between CPR and travel time has been verified in other studies (Alireza Fayazi and Vahidi 2018;

Yang 2017; Patel, Levin, and Boyles 2016; Elhenawy et al. 2015), indicating the derivation of an inverse relationship is consistent with the other findings in the literature.

6. Conclusion

In this study, the applicability of the BPR VDF to mixed-fleets and CAVs was investigated. Synthetic data was generated using 6600 modelling iterations. 30% of the synthetic data was used to assess the parameters of the BPR function. When it was found that the BPR function shows errors as CAV penetration or DoS increase, the same 30% of the data was used to generate a linear relationship between CPR, α and β . Using the remaining 70%, the predictive qualities of the recalibrated BPR function parameters were assessed. This assessment demonstrated that the RMSE improved from 15.16 to 8.86. In 67% of cases, the recalibrated variant better-predicted travel time than the traditional BPR function. Finally, of the 4620 simulation runs, forming the 70% of the dataset used for validation, the recalibrated BPR function better predicted travel time by 5.43 times.

Acknowledgements

The authors would like to acknowledge the assistance provided by the Research Centre for Integrated Transport Innovation (rCITI), School of Civil and Environmental Engineering, University of New South Wales (UNSW) Sydney, NSW 2052 Australia.

Disclosure statement

No potential conflict of interest was reported by the author(s).

ORCID

Hanna Grzybowska  <http://orcid.org/0000-0003-2614-5964>

Travis Waller  <http://orcid.org/0000-0002-2939-2090>

References

- Ahmed, Shofiq, Kakan Dey, and Ryan Fries. 2019. "Evaluation of Transportation System Resilience in the Presence of Connected and Automated Vehicles." *Transportation Research Record* 2673 (9): 562–574.
- Alireza Fayazi, Seyed, and Ardalan Vahidi. 2018. "Mixed-Integer Linear Programming for Optimal Scheduling of Autonomous Vehicle Intersection Crossing." *IEEE Transactions on Intelligent Vehicles* 3 (3): 287–299.
- Antoniottz, M., A. Deshpandez, and A. Giraultx. 1997. "Microsimulation Analysis of a Hybrid System Model of Multiple Merge Junction Highways and Semi-Automated Vehicles." *ITSC* 97: 147–152.
- Beza, Abebe Dress, and Mohammad Maghrour Zefreh. 2019. "Potential Effects of Automated Vehicles on Road Transportation: A Literature Review." *Transport and Telecommunication Journal* 20 (3): 269–278.
- Bureau of Public Roads. 1964. *Traffic Assignment Manual*. Washington: US Department of Commerce, Urban Planning Division.
- Bureau of Transport Statistics NSW. 2012. *BTS InfoSheet*.
- Chen, D., S. Ahn, M. Chitturi, and David A Noyce. 2017. "Towards Vehicle Automation: Roadway Capacity Formulation for Traffic Mixed with Regular and Automated Vehicles." *Transportation Research Part B: Methodological* 100: 199–221.
- Clements, L., and K. Kockelman. 2017. "Economic Effects of Automated Vehicles." *Transportation Research Record: Journal of the Transportation Research Board* 2606 (1): 106–114.
- Davidson, K. B. 1978. "A Flow-Travel Time Relationship for Use in Transportation Planning." *Australian Road Research* 8 (1): 32–35.
- Dervisoglu, G., G. Gomes, J. Kwon, R. Horowitz, and P. Varaiya. 2009. "Automatic Calibration of the Fundamental Diagram and Empirical Observations on Capacity." *Transportation Research Board 88th Annual Meeting*.
- Elhenawy, Mohammed, Ahmed A Elbery, Abdallah A Hassan, and Hesham A Rakha. 2015. "An Intersection Game-Theory-Based Traffic Control Algorithm in a Connected Vehicle Environment." *IEEE 18th International Conference on Intelligent Transportation Systems*. Las Palmas, 343–347.
- Epting, Shane. 2019. "Transportation Planning for Automated Vehicles – Or Automated Vehicles for Transportation Planning?" *Essays in Philosophy* 20 (2): 5.
- Ghiasi, A., O. Hussain, Z. Qian, and X. Li. 2017. "A Mixed Traffic Analysis and Lane Management Model for Connected and Automated Vehicles: A Markov Chain Method." *Transportation Research Part B: Methodological* 106: 2660292.

- Harper, C., C. Hendrickson, S. Mangones, and C. Samaras. 2016. "Estimating Potential Increases in Travel with Autonomous Vehicles for the Non-Driving, Elderly and People with Travel-Restrictive Medical Conditions." *Transportation Research Part C: Emerging Technologies* 72: 1–9.
- Heinrichs, D. 2016. "Autonomous Driving and Urban Land Use." *Autonomous Driving: Technical, Legal and Social Aspects*, 213–231.
- Hussain, O., A. Ghiasi, X. Li, and Z. Qian. 2016. *Freeway Lane Management Approach in Mixed Traffic Environment with Connected Autonomous Vehicles*. Vol. 77.
- Kamal, M., J. Imura, A. Ohata, T. Hayakawa, and K. Aihara. 2013. "Coordination of Automated Vehicles at a Traffic-Lightless Intersection 16th International IEEE Conference on Intelligent Transportation Systems (ITSC 2013).The Hague, Netherlands. 2013 October 6–9.
- Kaplan, E. L., and P. Meier. 1958. "Nonparametric Estimation from Incomplete Observations." *Journal of the American Statistical Association* 53 (282): 457–481.
- Katsaros, K., R. Kernchen, M. Dianati, D. Rieck, and C. Zinoviou. 2011. "Application of Vehicular Communications for Improving the Efficiency of Traffic in Urban Areas." *Wireless Communications and Mobile Computing* 11 (12): 1657–1667.
- Kesting, A., M. Treiber, M. Schonhof, and D. Helbing. 2008. "Adaptive Cruise Control Design for Active Congestion Avoidance." *Transportation Research Part C: Emerging Technologies* 16 (6): 668–683.
- Levin, M., and S. Boyles. 2016. "A Multiclass Cell Transmission Model for Shared Human and Autonomous Vehicle Roads." *Transportation Research Part C: Emerging Technologies* 62: 103–116.
- Manual, H.C. 2000. *Highway Capacity Manual*. Washington: Transportation Research Board, National Research Council.
- Mtoi, E., and R. Moses. 2014. "Calibration and Evaluation of Link Congestion Functions: Applying Intrinsic Sensitivity of Link Speed as a Practical Consideration to Heterogeneous Facility Types Within Urban Network." *Journal of Transportation Technologies* 4 (2): 141–149.
- Patel, Rahul, Michael W Levin, and Stephen D Boyles. 2016. "Effects of Autonomous Vehicle Behavior on Arterial and Freeway Networks." *Transportation Research Record* 2561 (1): 9–17.
- PTV Group. 2016. *PTV Vissim 9 User Manual*. Germany: PTV Group.
- Rakha, H., and B. Crowther. 2002. "Comparison of Greenshields, Pipes, and Van Aerde Car-Following and Traffic Stream Models." *Transportation Research Record* 1802 (1): 248–262.
- Saw, K., B. K. Katti, and G. Joshi. 2015. "Literature Review of Traffic Assignment: Static and Dynamic." *International Journal of Transportation Engineering* 2 (4): 339–347.
- Sinha, Amolika, Sai Chand, Kasun Wijayarathna, Navreet Virdi, and Vinayak Dixit. 2020a. "Comprehensive Safety Assessment in Mixed Fleets with Connected and Automated Vehicles: A Crash Severity and Rate Evaluation of Conventional Vehicles." *Accident Analysis & Prevention* 142: 105567.
- Sinha, Amolika, Sai Chand, Kasun Wijayarathna, Navreet Virdi, and Vinayak Dixit. 2020b. "Crash Severity and Rate Evaluation of Conventional Vehicles in Mixed Fleets with Connected and Automated Vehicles." *Procedia Computer Science* 170: 688–695.
- SIX Maps. 2021. *Western Distributor*. Sydney. <https://maps.six.nsw.gov.au/>.
- Spiess, H. 1990. "Technical Note – Conical Volume Delay Functions." *Transportation Science* 24 (2): 153–158.
- Talebpour, Alireza, and Hani S Mahmassani. 2016. "Influence of Connected and Autonomous Vehicles of Traffic Flow Stability and Throughput." *Transportation Research Part C* 71: 143–163.
- Tettamanti, T., I. Varga, and Z. Szalay. 2016. "Impacts of Autonomous Cars from a Traffic Engineering Perspective." *Periodica Polytechnica Transportation Engineering* 44 (4): 244–250.
- Transurban. 2020. *NSW Toll Road Data*. <http://nswtollroaddata.com>.
- Van Arem, Bart, Cornelie J. G. Van Driel, and Ruben Visser. 2006. "The Impact of Cooperative Adaptive Cruise Control on Traffic-Flow Characteristics." *IEEE Transactions on Intelligent Transportation Systems* 7 (4): 429–436.
- Van Den Berg, V. A., and E. T. Verhoef. 2016. "Autonomous Cars and Dynamic Bottleneck Congestion: The Effects on Capacity, Value of Time and Preference Heterogeneity." *Transportation Research Part B: Methodological* 94: 43–60.
- Virdi, Navreet. 2020. "Development of a Connected and Autonomous Vehicle Modelling Framework, with Implementation in Evaluating Transport Network Impacts and Safety." Doctoral dissertation, University of New South Wales.
- Virdi, Navreet, Hanna Grzybowska, T. Waller, and V. Dixit. 2019. "A Safety Assessment of Mixed Fleets with Connected and Autonomous Vehicles Using Surrogate Safety Assessment Module." *Accident Analysis & Prevention* 131: 95–111.
- Xiangjun, Q., J. Gregoire, A. D. Fortelle, and Fabien Moutarde. 2015. "Decentralized Model Predictive Control for Smooth Coordination of Automated Vehicles at Intersection." *European Control Conference*.
- Yang, Hang. 2017. *Scenarios Analysis of Autonomous Vehicles Deployment with Different Market Penetration Rate*. Maryland: University of Maryland.
- Ye, Lanhang, and Toshiyuki Yamamoto. 2018. "Modeling Connected and Autonomous Vehicles in Heterogeneous Traffic Flow." *Physica A: Statistical Mechanics and Its Applications* 490: 269–277.